Field Quality Measurements in a Single-Aperture 11 T Nb_3Sn Demonstrator Dipole for LHC Upgrades

N. Andreev, G. Apollinari, B. Auchmann, E. Barzi, R. Bossert, G. Chlachidze, J. DiMarco, M. Karppinen, F. Nobrega, I. Novitski, L. Rossi, D. Smekens, D. Turrioni, G. V. Velev, and A. V. Zlobin

***Abstract*—The upgrade of the Large Hadron Collider (LHC) collimation system foresees additional collimators in the LHC dispersion suppressor areas. The longitudinal space for the collimators could be provided by replacing some NbTi LHC main dipoles with shorter 11 T Nb_3Sn dipoles. To demonstrate this possibility, Fermilab and CERN have started a joint program to develop a Nb_3Sn dipole prototype suitable for installation in the LHC. The first step of this program is the development of a 2-m-long, 60-mm-bore, single-aperture demonstrator dipole with the nominal field of 11 T at the LHC operational current of 11.85 kA. This paper presents the results of magnetic measurements of the single-aperture Nb_3Sn demonstrator dipole including geometrical harmonics, coil magnetization, and iron saturation effects. The experimental data are compared with the magnetic calculations.**

***Index Terms*—Field quality, magnetic measurement, superconducting accelerator magnets.**

I. Introduction

THE planned upgrade of the Large Hadron Collider (LHC) collimation system requires additional collimators to be installed in the dispersion suppressor areas around points 2, 3 and 7 as well as around the high luminosity interaction regions [1]. Replacing some 8.33 T 15 m long NbTi LHC main dipoles (abbreviated MB) with shorter 11 T Nb_3Sn dipoles compatible with the accelerator lattice and the LHC main systems could provide the required longitudinal space for the collimators. These twin-aperture dipoles operating at 1.9 K and powered in series with the main dipoles should deliver the same integrated strength of 119 T • m at the operational current of 11.85 kA.

To demonstrate the feasibility of this approach, CERN and FNAL have started a joint R&D program to build a 5.5 m long twin-aperture Nb_3Sn prototype dipole for the collimation system upgrade [2]. The first phase of this program is the design, construction, and test of a 2 m long single-aperture demonstrator magnet, delivering approximately 11 T in a 60 mm bore at the LHC operational current of 11.85 kA with 20% margin.

Manuscript received October 8, 2012; accepted December 12, 2012. Date of publication January 3, 2013; date of current version March 8, 2013. This work was supported by the Fermi Research Alliance, LLC, under Contract DE-AC02-07CH11359 with the U.S. Department of Energy and European Commission under FP7 project HiLumi LHC, GA 284404.

N. Andreev, G. Apollinari, E. Barzi, R. Bossert, G. Chlachidze, J. DiMarco, F. Nobrega, I. Novitski, D. Turrioni, G. V. Velev, and A. V. Zlobin are with Fermi National Accelerator Laboratory, Batavia, IL 60510 USA (e-mail: zlobin@fnal.gov).

B. Auchmann, M. Karppinen, L. Rossi, and D. Smekens are with the European Organization for Nuclear Research, CERN CH-1211, Genève 23, Switzerland.

Color versions of one or more of the figures in this paper are available online at http://ieeexplore.ieee.org.

Digital Object Identifier 10.1109/TASC.2013.2237819

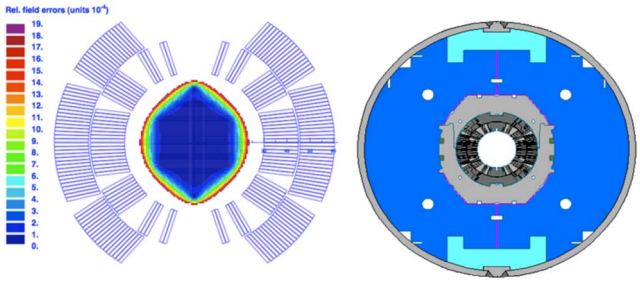

Fig. 1. Cross-sections of the coil (left) and the cold mass (right). The dark area in the coil aperture corresponds to relative field errors below 10^{-4}.

This paper presents the results of magnetic measurements and field analysis of the single-aperture Nb_3Sn demonstrator, and discusses the geometrical harmonics, coil magnetization and iron saturation effects. The demonstrator magnet was modeled with ROXIE [3] using properties of key structural materials [4]. Results of magnet quench performance and heater study are reported elsewhere [5], [6].

II. Magnet Design

The design details of the single-aperture demonstrator conceptual design are reported in [2], [7]. The coil cross-section was optimized for the double-aperture LHC iron yoke with separate collared coils and a 30-mm coil-yoke gap to provide a dipole field above 11 T at 11.85 kA, within ~20% margin on the load line at 1.9 K, and the low-order field errors below the 10^{-4} level (Fig. 1, left). The coil end spacers were optimized to minimize the integrated low-order field harmonics. The coil consists of 56 turns, 22 in the inner layer and 34 in the outer layer. The cable layer jump is integrated into the lead end spacer.

Both coil layers are wound from a single length of 40-strand keystoned 14.7 mm wide and 1.25 mm thick Rutherford cable [8] insulated with two layers of 0.075 mm thick and 12.7 mm wide E-glass tape. The cable is made of Nb_3Sn RRP-108/127, 0.7 mm in diameter, strand [9] and has a "twist-pitch" length of 125 mm. The strand nominal critical current density J_c (12 T, 4.2 K) is 2750 A/mm^2, the effective filament size D_{eff} is 55 μm and the Cu fraction is 53%.

The coils are surrounded by a multi-layer Kapton insulation and 316L stainless steel protection shells. They are placed inside the laminated collars made of high-Mn stainless steel. The collared coil is installed inside the vertically split 400 mm outer diameter yoke made of 1045 steel and fixed with aluminum clamps. The 12 mm thick 304L stainless steel shell provides final coil pre-compression and support up to the maximum

Fig. 2. PCB with both 26 and 130 mm long, 26 mm in diameter probes (top) and PSB probe holder (bottom). Typical probe rotational speed is 1 Hz.

design field of 12 T. Two 50 mm thick 304L stainless steel end plates welded to the shell restrict the longitudinal coil motion. The demonstrator dipole cross-section is shown in Fig. 1 (right). The details of magnet fabrication and its design parameters are reported in [5], [10].

III. Magnetic Measurement

Magnetic field in the aperture is expressed in terms of harmonic coefficients defined in a series expansion using the complex function formalism

$$B_y + iB_x = B_1 10^{-4} \sum_{n=1}^{\infty} (b_n + ia_n) \left(\frac{x+iy}{R_{ref}} \right)^{n-1} \quad (1)$$

where B_x and B_y in (1) are the horizontal and vertical field components in the Cartesian coordinates, b_n and a_n are the $2n$-pole normal and skew harmonic coefficients at the reference radius $R_{ref} = 17$ mm[11]. The right-handed measurement coordinate system is defined with the z-axis at the center of the magnet aperture and pointing from return to lead end.

The magnetic measurements were performed at the FNAL Vertical Magnet Test Facility. The demonstrator magnet was tested in the temperature range of 1.9–4.5 K. Most of the magnetic measurement results, presented in the paper, were taken at 4.5 K. Due to the limited quench performance the magnet did not reach the LHC nominal current of 11.85 kA and exhibited stable operation only at currents up to 7.5 kA at 4.5 K [5]. Therefore the maximum magnet current of 6.5 kA was used for the magnetic measurements described below.

For the measurements two printed circuit board probes (PCB) with the same diameter and a length of 130 mm and 26 mm, respectively, were used. The PCB probe technology was recently developed at FNAL [12]. The PCB probes and holder are shown in Fig. 2.

IV. Results and Analysis

A. Magnet Geometry, Persistent Current and Iron Saturation Effects

Table I summarizes the measured and simulated geometrical harmonics. The measured values are averaged over the 250 mm long tangential and 130 mm long PCB probes. The geometrical harmonics were determined at 3.5 kA current from 20 A/s loops to avoid the ramp-rate compensation issues as well as the persistent and eddy current effects. The calculated harmonics include two cases: "design" dipole geometry optimized with ROXIE code, and "as-built" geometry calculated with ROXIE using input from ANSYS. The disagreement between measured and calculated "as-built" harmonics is quite large and it needs to be understood, especially in the normal sextupole and low order skew multipoles.

TABLE I
Calculated and Measured Geometrical Harmonics

b_n a_n	Design*	As-Built**	Measured***
b_2	0.00	1.14	-0.50±0.05
b_3	0.21	1.07	6.38±0.18
b_4	0.00	-0.18	0.02±0.16
b_5	0.88	0.30	-0.73±0.02
b_6	0.00	-0.03	2.46±1.40
a_2	0.00	-0.07	-1.43±1.18
a_3	0.00	2.38	4.67±0.05
a_4	0.00	0.24	-2.50±0.24
a_5	0.00	0.80	1.46±0.37
a_6	0.00	0.01	-2.32±0.03

* ROXIE optimization
** ROXIE+ANSYS including the assembly errors and cross-section deformations
*** RMS uncertainties; the systemic uncertainty is estimated to be on the level of 0.5 units.

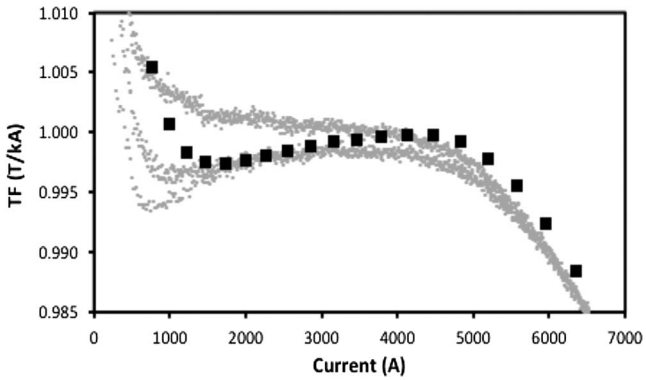

Fig. 3. Measured (points) and calculated (squares) transfer function TF. Calculated data correspond to current ramp up. Measurements using 26-mm PSB probe at 4.5 K.

Fig. 3 shows the measured and simulated variations of the dipole transfer function $(TF = B_1/I)$ versus the excitation current. The current loop was executed from 0 to 6.5 kA with 20 A/s ramp rate at 4.6 K. Fig. 4 shows the sextupole (b_3), and dodecapole (b_5) field harmonics measured at the same condition (top and bottom plots respectively). The filled squares in Figs. 3 and 4 represent the calculated values. They were computed using realistic, "as-built", magnet cross-section (including the shims used to achieve the coil target pre-stress), with the persistent current and iron saturation effects. The latter is seen in the TF and b_3 plots at currents over 4.5 kA, and is quite well predicted by the simulation.

The significant persistent current effect, seen at low currents in the TF and b_3, b_5 field harmonics, is due to large D_{eff} and J_c of the Nb_3Sn strand [13]. The experimental results are in a good agreement with calculations at currents above 2 kA after coil re-magnetization. The simulation of the re-magnetization effect below 2 kA requires improvement of the superconductor magnetization model in magnet coil.

B. Current Reset Effect

Fig. 5 shows the b_3 harmonic hysteresis loops at different reset currents (the lowest current in the magnet during the operation). The LHC injection current 760 A is represented

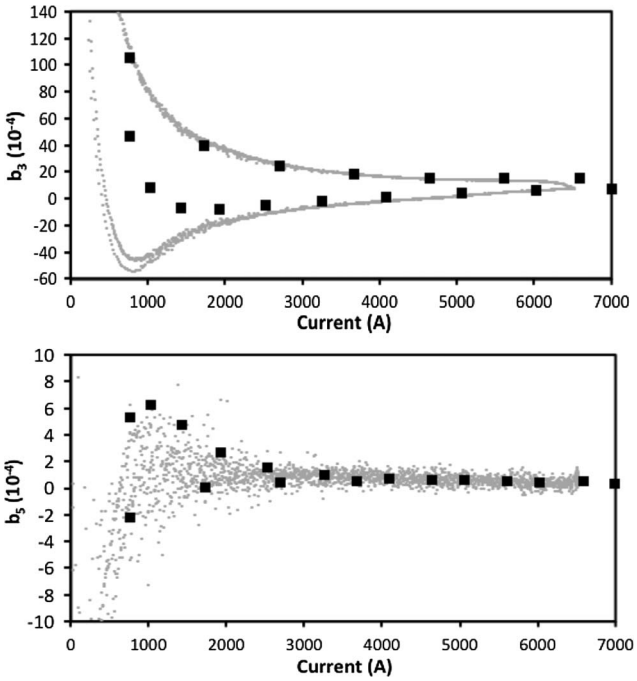

Fig. 4. Measurements (points) and simulation (squares) of the allowed harmonics b_3 (upper plot) and b_5 (lower plot). Measurements using 26-mm PSB probe at 4.5 K.

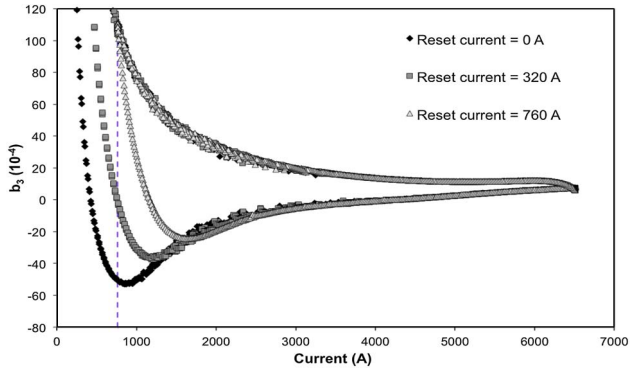

Fig. 5. Sextupole variation versus magnet current for various pre-cycle reset currents. Measurements using 130-mm PSB probe at 4.5 K.

by the vertical dashed line. Due to the large re-magnetization effect in the Nb_3Sn coils, the b_3 at injection strongly depends on the reset current. This plot also shows that even for the RRP-108/127 strand used in the demonstrator dipole, with the reset current close to zero (100 A presently), the minimum on the b3 curve is relatively close to the LHC injection current."

A LHC current profile with a low reset current will significantly simplify the sextupole correction for the 11 T Nb_3Sn dipole during the ramp between the injection and collision points due to the monotonic behavior of the sextupole field component in the region of interest. It also suggests that RRP-108/127 strand could be considered for use in production magnets for the LHC collimation system upgrade.

C. Eddy Current Effect

To estimate the effect of the eddy currents on the magnet transfer function and the field quality of the single-aperture

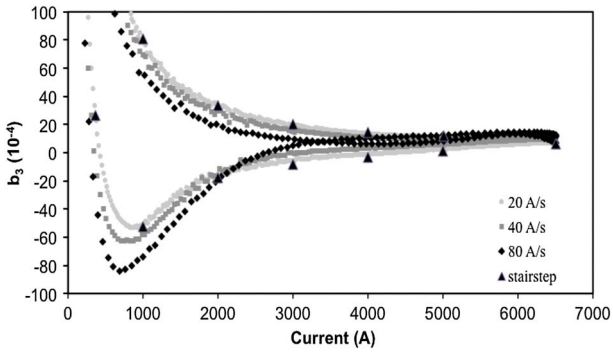

Fig. 6. Normal sextupole b_3 field component loops executed at ramp rate of 20 A/s, 40 A/s, and 80 A/s at 4.5 K. The points represent the "stair step" measurement.

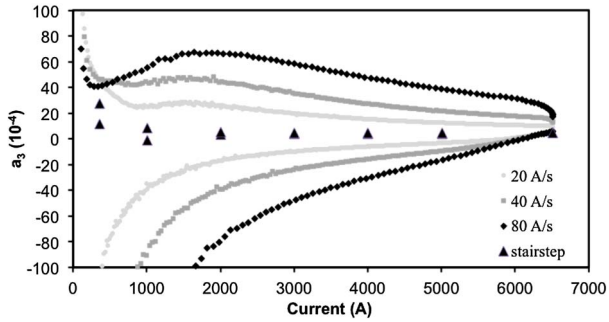

Fig. 7. Skew sextupole a_3 field component loops executed at ramp rate of 20 A/s, 40 A/s, and 80 A/s at 4.5 K. The points represent the "stair step" measurement.

demonstrator, several excitation loops have been executed at ramp rates of 20 A/s, 40 A/s, and 80 A/s.

Fig. 6 shows the corresponding normal sextupole (b_3) field loops. The dots represent the b_3 in "stair-step" current profile measurement with duration at every current step of 120 s. These measurements represent the ramp rate of 0 A/s. To minimize the effect of the eddy currents on the "stair-step" test, the measurement was executed with a ramp rate of 10 A/s. The result shows a relatively small dependence of the sextupole loops on the current ramp rate.

The result for the skew sextupole (a_3) field loops is shown in Fig. 7. Surprisingly, a large increase of the a_3 loop width is observed. Similar effect is seen in the other allowed and unallowed field harmonics. This effect needs additional investigation and could be explained with unbalanced currents induced in few turns in the magnet coils due to current ramp.

The observed increase of the TF width at 2 kA from 20 to 80 A/s was less than 2%.

D. Long-Term Dynamic Effects

Long-term dynamic effects in superconducting magnets are usually associated with the decay of the allowed field components at injection, which is followed by a subsequent snapback during the acceleration ramp [14], [15].

To investigate these effects in the single-aperture demonstrator dipole, measurements with an accelerator current profile similar to the one used at the LHC magnets but with lower maximum current of 6.5 kA were performed. The duration of

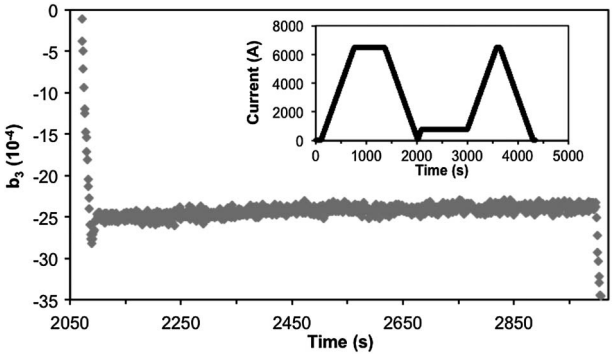

Fig. 8. Current profile of the accelerator cycle (inset) and normal sextupole variation versus time during the simulated injection plateau.

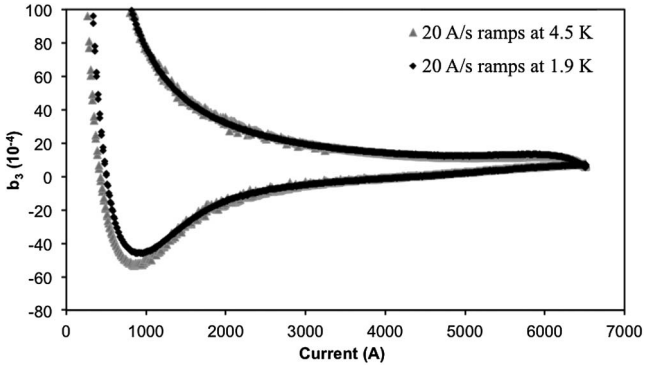

Fig. 9. Comparison of the sextupole field component measured at 1.9 and 4.5 K for 20 A/s current ramp. Measurements using 130 mm PSB probe.

the injection plateau was set to ~900 s. The decay and snapback in the normal sextupole component (b_3) is shown in Fig. 8 (the inset shows the executed current profile).

A typical decay and snapback behavior was not observed in the magnet. A slow linear drift of approximately 2 units is measured without a subsequent snapback (Fig. 8). A typical exponential long-term decay and snap-back was not observed also in Nb_3Sn dipole model magnets previously made at Fermilab [16]. In comparison, average amplitude in the NbTi LHC dipoles was found to be at the same order of 2 units with a well-defined snapback of several seconds [14].

E. Effect of Temperature

The operational temperature of LHC magnets is 1.9 K. To investigate the effect of temperature on field harmonics a set of magnetic measurements were executed at 1.9 K. Fig. 9 shows the comparison of the sextupole field (b_3) measured at 4.5 and 1.9 K. In the current interval from 1 to 2 kA, the simulation predicts approximately 7% increase of the width of the hysteresis loop at 1.9 K due to higher critical current density J_c. Instead, 3% decrease in the hysteresis width was observed. This discrepancy needs a future investigation.

V. Conclusion

Magnetic measurements and analysis were performed for the 2 m long single-aperture demonstrator dipole including geometrical, coil magnetization and iron saturation effects.

The design geometrical field harmonics in the magnet body are small due to coil cross-section optimization. However, some measured low order harmonics are quite large due to the imperfect "as-built" coil geometry. The level of geometrical harmonics will be reduced in the future by optimizing the coil geometry taking into account the above effects.

The iron saturation effect in the single-aperture configuration is well understood.

The coil magnetization effect is relatively large at the LHC injection level due to the high J_c and large D_{eff} of the Nb_3Sn strand used in the demonstrator magnet. This effect could be reduced by utilizing a strand with smaller D_{eff} and passive correction schemes. The eddy current effect is also relatively large in some non-allowed harmonics. This phenomenon needs to be understood. Practically this effect will be suppressed by using a cable with resistive core. A next short dipole model with RRP-150/169 strand and cored cable will be tested next year.

As expected from the previous measurements of the Nb_3Sn magnets [16], the long-term dynamic effects in the normal sextupole component was estimated to be small.

Acknowledgment

The authors thank the technical staff of FNAL Technical Division for contributions to magnet design and fabrication.

References

[1] L. Bottura *et al.*, "Advanced accelerator magnets for upgrading the LHC," *IEEE Trans. Appl. Supercond.*, vol. 22, no. 3, p. 4002008, Jun. 2012.
[2] A. V. Zlobin *et al.*, "Development of Nb3Sn 11 T single aperture demonstrator dipole for LHC upgrades," in *Proc. PAC*, NYC, 2011, p. 1460.
[3] ROXIE Code for an Electromagnetic Simulation and Optimization of Accelerator Magnets. [Online]. Available: http://cern.ch/roxie
[4] B. Auchmann *et al.*, "Field quality analysis of a single-aperture 11 T Nb3Sn demonstrator dipole for LHC upgrades," presented at the IPAC, New Orleans, LA, 2012.
[5] A. V. Zlobin *et al.*, "Development and test of a single-aperture 11 T Nb3Sn demonstrator dipole for LHC upgrades," *IEEE Trans. Appl. Supercond.*, vol. 23, 2013, to be published.
[6] G. Chlachidze *et al.*, "Quench protection study of a single-aperture 11 T Nb3Sn demonstrator dipole for LHC," *IEEE Trans. Appl. Supercond.*, vol. 23, 2013, to be published.
[7] A. V. Zlobin *et al.*, "Design and fabrication of a single-aperture 11 T Nb3Sn dipole model for LHC upgrades," *IEEE Trans. Appl. Supercond.*, vol. 22, no. 3, p. 4001705, Jun. 2012.
[8] E. Barzi *et al.*, "Development and fabrication of Nb3Sn rutherford cable for the 11 T DS dipole demonstration model," *IEEE Trans. Appl. Supercond.*, vol. 22, no. 3, p. 6000805, 2012.
[9] M. B. Field *et al.*, "Internal Tin Nb_3Sn conductors for particle accelerator and fusion applications," *Adv. Cryog. Eng.*, vol. 54, p. 237, 2008.
[10] A. V. Zlobin *et al.*, "Status of a single-aperture 11 T Nb_3Sn demonstrator dipole for LHC upgrades," in *Proc. IPAC*, New Orleans, 2012, p. 1098.
[11] A. Jain, "Basic theory of magnets," in *Proc. CERN Accel. School*, Anacapri, Italy, 1997, pp. 1–26, CERN-98-05.
[12] J. DiMarco *et al.*, "Application of PCB and FDM technologies to magnetic measurement probe system development," *IEEE Trans. Appl. Supercond.*, vol. 23, 2013, to be published.
[13] E. Barzi *et al.*, "Studies of Nb_3Sn strands based on the restacked-rod process for high-field accelerator magnets," *IEEE Trans. Appl. Supercond.*, vol. 22, no. 3, p. 6001405, Jun. 2012.
[14] N. Sammut *et al.*, "Mathematical formulation to predict the harmonics of the superconducting large hadron collider magnets: II. dynamic field changes and scaling laws," *Phys. Rev. Spec. Top. Accel. Beams*, vol. 10, 2007.
[15] G. V. Velev *et al.*, "Measurements of the persistent current decay and snapback effect in tevatron dipole," *IEEE Trans. Appl. Supercond.*, vol. 17, no. 2, pp. 1105–1108, Jun. 2007.
[16] G. V. Velev *et al.*, "Measurements of the persistent current decay and snapback effect in Nb_3Sn accelerator prototype magnets at Fermilab," in *Proc. IPAC*, New Orleans, 2012, p. 3593.